A Boltzmann Transport Equation Model for Substrate Damage During Focused Helium Ion Beam Fabrication of Nanostructures

Qi Li
Dept. of Mechanical Engineering
Southeast University
Nanjing, China
230208023@seu.edu.cn

Ye Chen
Dept. of Mechanical Engineering
Southeast University
Nanjing, China
chenyenj@qq.com

Yan Xing
Dept. of Mechanical Engineering
Southeast University
Nanjing, China
xingyan@seu.edu.cn

***Abstract*—In this work, a Boltzmann transport equation model is proposed for the substrate damage simulation during focused helium ion beam processing. The model links the helium ion moderation, cascade collisions and lattice displacement. The travels of helium and displaced atoms are described by the transport equations for helium ions and displaced atoms, respectively, which are the core of the model. The main outputs of the equation model solved by a deterministic method include the spatial and temporal distribution of the helium ions, the energy transfer information and the spatial and temporal distribution of deposited point defects which directly reflects the substrate damage. The model has the advantage of being fully informative, accurate and efficient compared to existing methods. The comparisons between simulation results and experiments conducted on silicon and silicon carbide prove that the proposed model can effectively and accurately simulate substrate damage during focused helium ion beam processing.**

Keywords—Focused helium ion beam, Boltzmann transport equation, Ion implantation damage, Amorphous profile, Defect distribution

I. INTRODUCTION

Focused helium ion beams (helium FIB) as an emerging nanoscale processing method with high resolution can be applied to many fields such as mask repair [1], ion beam-induced nanostructure deposition [2,3] and helium ion implanted nanostructures [4]. However, due to the low sputtering and diffusion rates of helium ions, helium FIB processing of bulk materials is associated with unique substrate damage phenomena that differ from widely used gallium beams, such as amorphization [5] of the material, swelling, and the appearance of helium bubbles [6]. Helium implantation damage in the substrate during beam processing has its advantages and disadvantages [7,8], and while having many detrimental effects on the performance of the prepared devices, it can also be an effective means of material modification processes. Therefore, helium implantation-induced substrate damage is an important object in experimental and simulation studies of helium FIB, and a comprehensive model is needed to capture and link the ion implantation damage stage during helium FIB processing.

Currently, the vast majority of computer simulation methods applied to the study of helium FIB processes are based on the Monte Carlo method [9] and molecular dynamics method [10]. One of the most widely accepted methods is the SRIM (Stopping Range of Ions in Matter) software [11] based on binary collisions and the Monte Carlo method, which has been used by many researchers to obtain the defects distribution and sputtering yield of FIB processing [12-14]. However, since the Monte Carlo method is essentially a method for tracking the states of individual particle, the simulation accuracy increases with the number of simulated particles while the computer resources occupied by the simulation will also increase geometrically [15]. The molecular dynamics method simulations are even less capable of simulating damage structures of several hundred nanometers. Therefore, the existing simulation methods are not capable of simulating helium FIB processing with both accuracy and efficiency.

In this paper, a Boltzmann transport equation model (BTEM) based on particle transport theory is developed to describe the travel of ions and atoms in the substrate during helium FIB processing. The use of the published sophisticated deterministic method [16] to solve Boltzmann transport equations makes the computational efficiency of the model no longer affected by the number of simulated particles, and the description of particles by the equation in the full range including temporal, spatial, velocity, and direction of motion also ensures the accuracy and precision of the model. The model was validated by comparing the calculated amorphous damage profiles with transmission electron microscope (TEM) images obtained from focused helium ion beam processing experiments on silicon and silicon carbide (SiC) [16,17]. The model was then used to simulate the damaged structure at different ion doses and beam energies, and to analyze the effect of process parameters on the damaged structure and thus guiding focused helium ion beam fabrication of nanostructures.

II. BOLTZMANN TRANSPORT EQUATION MODEL

BTEM proposed in this work consists of two parts: the transport of injected helium ions and the cascade collision initiated by primary knock-on atoms.

A. Transport of injected helium ions

The transport process of injected helium ions in substrate is described by a Boltzmann transport equation for helium ions (BTE (He)) which could be written as:

$$\frac{\partial \phi_i}{\partial t} + \boldsymbol{v} \cdot \nabla_{\mathrm{r}} \phi_i = Q_S \{\phi_i\} \ . \tag{1}$$

Here, $\phi_i(\mathbf{r}, E, \boldsymbol{\Omega}, t)$ is a distribution function describing the energy E, spatial $\mathbf{r}$, motion direction $\boldsymbol{\Omega}$ and temporal t evolution of helium ions, and $\boldsymbol{v}$ denotes the ion velocity. Q_S refers to the scattering operator,

XXX-X-XXXX-XXXX-X/XX/$XX.00 ©20XX IEEE

$$Q_S\{\phi_i\} = \iint v'\phi_i(\mathbf{r},E',\boldsymbol{\Omega}',t)\mu_{ela}(E',\boldsymbol{\Omega}'\to E,\boldsymbol{\Omega})d\boldsymbol{\Omega}'dE' + \iint v'\phi_i(\mathbf{r},E',\boldsymbol{\Omega}',t)\mu_{ine}(E',\boldsymbol{\Omega}'\to E,\boldsymbol{\Omega})d\boldsymbol{\Omega}'dE' - v\mu_{total}(E)\phi_i(\mathbf{r},E,\boldsymbol{\Omega},t), \quad (2)$$

the first and second terms on the right represent the generation of ions with energy E moving in the direction $\boldsymbol{\Omega}$ by the elastic scattering between the particles and the nucleus and the inelastic scattering between the particles and the electron cloud, respectively, and the last term represents the ion loss due to elastic as well as inelastic scattering. μ in this paper, with different subscripts represents cross section for different scattering processes.

After solving (1) deterministically [16], in addition to the temporal-spatial distribution of helium ions obtained as

$$n_i(\mathbf{r},E,t) = \frac{1}{v}\int \phi_i(\mathbf{r},E,\boldsymbol{\Omega},t)\,d\boldsymbol{\Omega}, \quad (3)$$

two important transport results can be obtained: the distribution of the energy transferred through elastic collisions between ions and target atoms T_{dam} and the source term of primary knock-on atoms Q_{PKA}, which can be obtained by (4) and (5).

$$T_{dam}(\mathbf{r},t) = \iint (E-E')\phi_i(\mathbf{r},E,\boldsymbol{\Omega},t)\mu_{ela}(E,\boldsymbol{\Omega}\to E',\boldsymbol{\Omega}')dE'd\boldsymbol{\Omega}'d\boldsymbol{\Omega}dE, \quad (4)$$

$$Q_{PKA} = \iint v'\phi_i(\mathbf{r},E',\boldsymbol{\Omega}',t)\mu_{PKA}(E',\boldsymbol{\Omega}'\to E,\boldsymbol{\Omega})d\boldsymbol{\Omega}'dE'. \quad (5)$$

B. Cascade collision of displaced atoms

The helium ions undergo elastic collisions and produce primary displaced atoms and the primary displaced atoms undergo elastic collisions and produce higher generations of displaced atoms. This process is called cascade collision and could be described by the transport equation of displaced atoms (BTE (da)):

$$\frac{\partial\phi_{da}}{\partial t} + \boldsymbol{v}\cdot\nabla_{\mathbf{r}}\phi_{da} = Q_S\{\phi_{da}\} + Q_C\{\phi_{da}\} + Q_{PKA}. \quad (6)$$

ϕ_{da} is a distribution function describing the state of displaced atoms, and there is an additional source term $Q_C\{\phi_{da}\}$ in (6) representing the generation of higher generation displaced atoms compared to (1),

$$Q_C\{\phi_{da}\} = \iint v''\phi_{da}(\mathbf{r},E'',\boldsymbol{\Omega}'',t)\mu_{cas}(E'',\boldsymbol{\Omega}''\to E,\boldsymbol{\Omega})d\boldsymbol{\Omega}''dE''. \quad (7)$$

and Q_{PKA} calculated by (5) could be a source term of the primary displaced atoms or transferred to be the initial condition of (6). The solution of (6) gives direct information on the substrate damage since the creation of a displaced atom represents the occurrence of a damage event (lattice displacement).

The sketch of BTEM is shown in Fig. 1. As we can summarize from Fig. 1, the core of BTEM is the two BTEs, which describe the transport of incident helium ions and cascade collisions, respectively, and the two BTEs are linked by the primary displaced atoms produced by the collision of helium ions and substrate atoms and the transport results of both can reflect the damage of the substrate in their way, which is the goal of BTEM simulation.

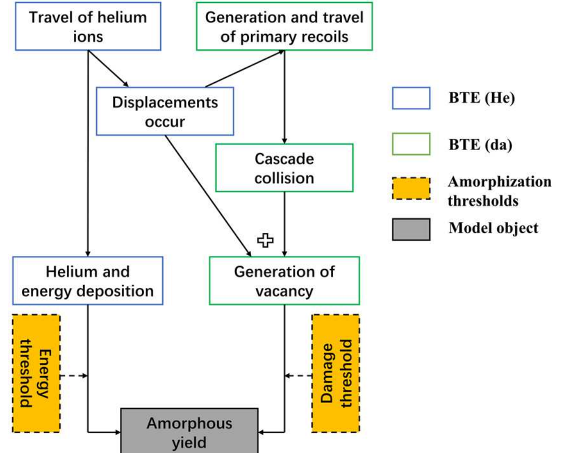

Fig. 1 Sketch of BTEM for substrate damage during helium FIB processing.

III. Results and Discussion

A. Key outputs of the transport equation of helium ions

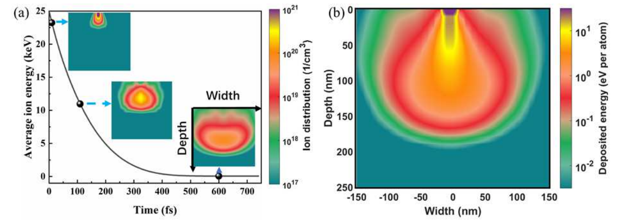

Fig. 2 (a) Simulation results of the average energy carried by ions over time, accompanied by the distributions of helium ions at different time points; (b) BTEM simulation result of the energy deposited in per lattice site of the target due to the elastic collisions between ions and target atoms. The substrate is SiC, the beam energy is 25 keV and ion dose is 10^{16}ions/cm^2.

As mentioned earlier, the key outputs of BTE (He) include the temporal-spatial distribution of helium ions and the distribution of the energy transferred through elastic collisions, which are shown in Fig. (2). As can be seen in Fig. 2(a), the average energy carried by the ions decreases with time and most of the energy loss occurs within the initial 200 femtoseconds, and the entire ion moderation process is completed within 1 picosecond, which is consistent with the literature [18]. Meanwhile, the distribution range of helium ions is increasingly broad with time both in depth and radial direction. Fig. 2(b) shows the energy distribution deposited in the substrate lattice for a beam energy of 25 keV and ion dose of 10^{16}ions/cm^2 obtained from BTEM simulation with SiC as the target material. It can be seen that the peak of the deposition energy is at the surface and the contour evolution of the deposition energy from high to low is developed first in depth and then in radial direction. The energy deposited in the substrate lattice due to elastic collisions between ions and target atoms can be proportionally converted to the damage energy causing the final substrate damage [19] and the distribution of vacancies can be further calculated

B. *Key outputs of the transport equation of displaced atoms*

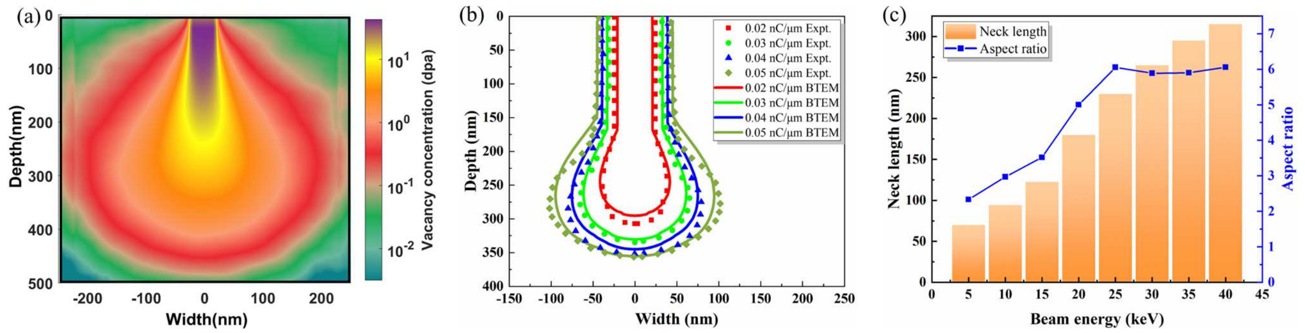

Fig. 3 (a) BTEM simulation result of the displacement damage distribution in silicon at a beam energy of 35 keV with an ion dose of 0.04 nC/μm; (b) Comparisons of BTEM simulation and experimental results [16] of the amorphous profile of silicon treated with helium FIB at a beam energy of 35 keV. (c) BTEM simulation results of depth and depth-to-width ratio of amorphous structures in silicon during He-FIB process with low ion doses.

The displacement damage (vacancy) distribution calculated by BTEM that can be used to determine the amorphous threshold energy is given in Fig. 3. It can be seen that the distribution of the vacancies has a similar contouring trend to the deposition energy distribution in Fig. 2(b). As shown in Fig. 3(b), the simulation results of the substrate displacement damage can be used simultaneously to predict the amorphous profile at several different ion doses by extracting the corresponding contour profile. The amorphization thresholds of silicon is chosen to be around 3 dpa (displacement per atom) and the simulation results are in good agreement with the experimental results. In addition, with the help of BTEM, the highest depth-to-width ratio of the amorphous structure formed at different beam energies can be simulated, which is important for the design and study of the amorphous modification of materials. As shown in Fig. 3(c), the depth of the amorphous region continues to increase with the beam energy, and the depth-to-width ratio continues to increase with the beam energy at beam energies less than 25 keV, however, there exists a maximum value of about 6 for the depth-to-width ratio.

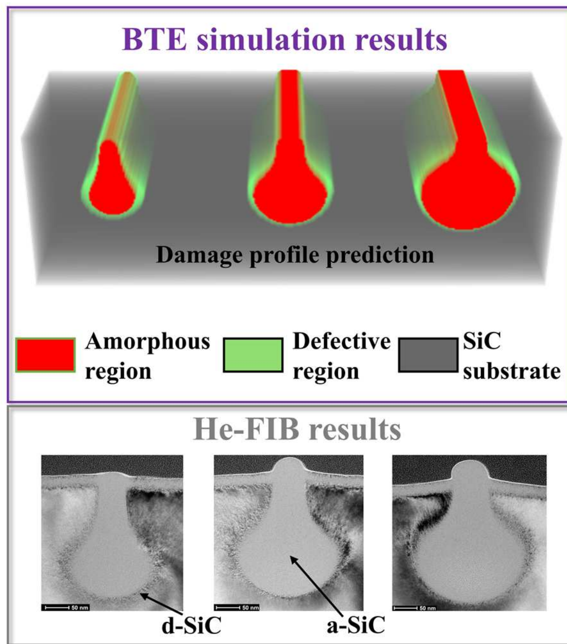

Fig. 4 Model predictions for the He-FIB line-scan process and corresponding cross-sectional TEM images of SiC [17].

National Natural Science Foundation of China

Based on the simulation results of the distribution of lattice displacements, the damage morphology of the substrate could be predicted and visualized in 3D with the object-oriented Visualization Toolkit (VTK) [20]. The model predictions for the helium FIB line-scan process and the corresponding experimental images are given in Fig. 4. It can be seen that the BTEM simulation results on substrate damage can provide an effective prediction of the damage pattern of the substrate in helium FIB processing

C. *Comparison of BTEM and SRIM*

As mentioned in the previous section, solving the transport equations deterministically gives BTEM multiple advantages over SRIM software. A comprehensive comparison of the simulation results of BTEM and SRIM in terms of computational efficiency, computational accuracy, and accuracy of results is presented in Fig. 5.

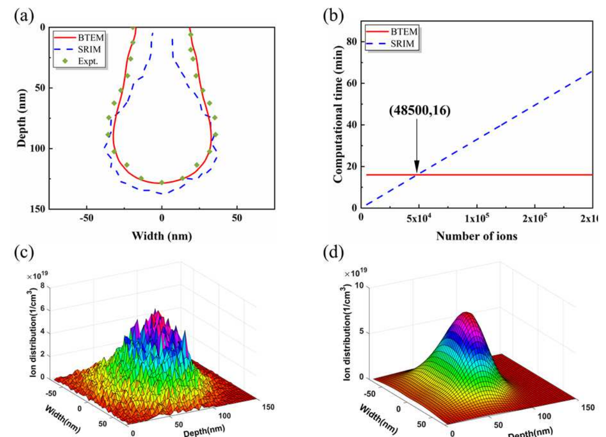

Fig. 5 (a) Comparison of damage profiles of BTEM simulation and SRIM simulation; (b) The computational times of BTEM and SRIM with the number of computed particles; (c)-(d) Results of BTEM and SRIM simulations of helium ion distribution with the same computational time (c) SRIM, (d) BTEM; The hardware conditions, beam energy (10 keV), ion dose (10^{16} ions/cm^2) and substrate (silicon) are the same for both simulations.

First, the accuracy, as shown in Fig. 5(a), the amorphous profile simulated by BTEM is closer to the experimental profile than the SRIM simulation. Then comes the computational efficiency, as shown in Fig. 5(b), the computational time for BTEM is independent of the number of ions simulated because the ion dose is a parameter that does not need to be discretized in BTEM, while the calculation time for SRIM is linearly related to the number of ions because SRIM tracks the ions one by one. And the

computation time curves of BTEM and SRIM in Fig. 5(b) have an intersection point (48500 ions,16 min). Results of SRIM and BTEM simulation results of the helium ion distribution with the same computational time are shown in Fig. 5(c) and 5(d), respectively. As can be seen that the simulation results of BTEM are smoother and more continuous than those of SRIM, which means that BTEM has higher computational accuracy for simulation needs with rare events and precise requirements.

IV. Conclusion

In this study, a computational model of substrate damage during focused helium ion beam nanofabrication was developed based on the Boltzmann transport equations. With this model important transport results are obtained, such as spatial and temporal distributions of helium ions, energy transport information and spatial and temporal distributions of deposited defects. The overall dimensions of the amorphous profile extracted from the final vacancy distribution are in good agreement with experimental observations. The key dimensions of the defective structures for different process parameters are also predicted and analyzed to obtain the dependence of the structure dimensions on beam energy and ion dose. The computational accuracy of the Boltzmann transport equation method is not affected by the number of simulated particles and is higher than that of the SRIM simulation method in the same computational time.

Acknowledgment

This work was supported by the National Natural Science Foundation of China (Grant No.51875104).

References

[1] C.M. Gonzalez, W. Slingenbergh, R. Timilsina, J.-H. Noh, M.G. Stanford, B.B. Lewis, K.L. Klein, T. Liang, J.D. Fowlkes, P.D. Rack, Evaluation of mask repair strategies via focused electron, helium, and neon beam induced processing for EUV applications, in: Extrem. Ultrav. Lithogr. V, SPIE, 2014: p. 90480M.

[2] P.F.A. Alkemade, H. Miro, Focused helium-ion-beam-induced deposition, Appl. Phys. A Mater. Sci. Process, vol. 117, pp. 1727–1747, 2014.

[3] P. Chen, E. Van Veldhoven, C.A. Sanford, H.W.M. Salemink, D.J. Maas, D.A. Smith, P.D. Rack, P.F.A. Alkemade, Nanopillar growth by focused helium ion-beam-induced deposition, Nanotechnology, vol. 21, no. 45, 2010.

[4] C.S. Kim, R.G. Hobbs, A. Agarwal, Y. Yang, V.R. Manfrinato, M.P. Short, J. Li, K.K. Berggren, Focused-helium-ion-beam blow forming of nanostructures: Radiation damage and nanofabrication, Nanotechnology, vol. 31, no. 4, 2020.

[5] M.G. Stanford, B.B. Lewis, V. Iberi, J.D. Fowlkes, S. Tan, R. Livengood, P.D. Rack, In Situ Mitigation of Subsurface and Peripheral Focused Ion Beam Damage via Simultaneous Pulsed Laser Heating, Small, vol. 12, pp. 1779–1787, 2016.

[6] F.I. Allen, P. Hosemann, M. Balooch, Key mechanistic features of swelling and blistering of helium-ion-irradiated tungsten, Scr. Mater., vol. 178, pp. 256–260, 2020.

[7] G. Hlawacek, V. Veligura, R. van Gastel, B. Poelsema, Helium ion microscopy, J. Vac. Sci. Technol. B, vol. 32, pp. 20801, 2014.

[8] F.I. Allen, A review of defect engineering, ion implantation, and nanofabrication using the helium ion microscope, Beilstein J. Nanotechnol., vol. 12, pp. 633–664, 2021.

[9] K. Ohya, Molecular dynamics and dynamic Monte-Carlo simulation of irradiation damage with focused ion beams, in: Metrol. Insp. Process Control Microlithogr. XXXI, SPIE, vol. 10145, pp. 101451V, 2017.

[10] Z. Tong, X. Luo, Investigation of focused ion beam induced damage in single crystal diamond tools, Appl. Surf. Sci., vol. 347, pp. 727–735, 2015.

[11] J.F. Ziegler, M.D. Ziegler, J.P. Biersack, SRIM - The stopping and range of ions in matter (2010), Nucl. Instruments Methods Phys. Res. Sect. B Beam Interact. with Mater. Atoms, vol. 268, pp. 1818–1823, 2020.

[12] R. Timilsina, S. Tan, R. Livengood, P.D. Rack, Monte Carlo simulations of nanoscale focused neon ion beam sputtering of copper: Elucidating resolution limits and sub-surface damage, Nanotechnology, vol. 25, no. 48, 2014.

[13] R. Timilsina, P.D. Rack, Monte Carlo simulations of nanoscale focused neon ion beam sputtering, Nanotechnology, vol. 24, no. 49, 2013.

[14] C.W. Yang, C. Chou, W.C. Chen, H.H. Lin, A single nano-void precisely positioned in SiO2/Si substrate by focused helium ion beam technique, Vacuum, vol. 152, pp. 188–192, 2018.

[15] K. Rupp, C. Jungemann, S.M. Hong, M. Bina, T. Grasser, A. Jüngel, A review of recent advances in the spherical harmonics expansion method for semiconductor device simulation, J. Comput. Electron, vol. 15, pp. 939–958, 2016.

[16] Q. Li, X.H. Lin, C. Zhang, Q. Chen, T. Shao, Y. Xing, Damage profile evolution model based on the Boltzmann transport equation for silicon micromachining with the focused helium ion beam, Sensors Actuators, A Phys., vol. 328, 112802, 2021.

[17] Q. Chen, M.A. Gosalvez, Q. Li, Y. Xing, Helium focused ion beam induced subsurface damage on Si and SiC substrates: Experiments and generative deep neural network modeling via position-dependent input, J. Mater. Res. Technol., vol. 24, pp. 3363-3382, 2023.

[18] V. Krsjak, J. Degmova, S. Sojak, V. Slugen, Effects of displacement damage and helium production rates on the nucleation and growth of helium bubbles – Positron annihilation spectroscopy aspects, J. Nucl. Mater., vol. 499. pp. 38–46, 2018.

[19] R.E. Stoller, M.B. Toloczko, G.S. Was, A.G. Certain, S. Dwaraknath, F.A. Garner, On the use of SRIM for computing radiation damage exposure, Nucl. Instruments Methods Phys. Res. Sect. B Beam Interact. with Mater. Atoms, vol. 310. pp. 75-80, 2013.

[20] W.J. Schroeder, L.S. Avila, W. Hoffman, Visualizing with VTK: A tutorial, IEEE Comput. Graph. Appl., vol. 20, pp. 20–27, 2000.